International Workshop on Thermal Forming and Welding Distortion, 6th-7th of April 2011, Bremen, Germany, pages 169-179

Modelling distortion reduction on pre- and post-weld rolled gas metal arc welded plates

L. D. Cozzolino[1], H. E. Coules[1], P. A. Colegrove[1], S. W. Wen[2]

1. Cranfield University, Cranfield, Bedfordshire, MK43 0AL, UK
2. Tata Steel Europe, Swinden Technology Centre, Rotherham, South Yorkshire S60 3AR, UK

Residual stress generated during welding can cause distortion, especially when applied on relatively thin plates. There are several standard and well documented techniques to reduce distortion and residual stress after welding, however these techniques are often costly and time consuming to implement on an industrial scale. In this paper we demonstrate the pre- and post-weld rolling techniques for reducing weld distortion. Pre-Weld Rolling (PWR) can be applied before fabrication, potentially by the steel manufacturer. An experimental investigation indicated that there was an average 38% reduction of distortion with this technique. Finite element analysis (FEA) was used to determine the stress distribution to understand the phenomenon. A number of conditions were analysed, including rolling on the top (weld bead side, Figure 1) and bottom (weld root side) surfaces at different distances from the edge where the material was subsequently welded. Both experimental and numerical results have shown that rolling on the bottom side gives better results in terms of distortion reduction. In addition the likely mechanism is the addition of stresses due to rolling which counteract those induced by welding. Some preliminary experimental results on post-weld rolling show that this is a more effective method for reducing distortion, producing virtually flat plates. This significant finding has the potential to eliminate distortion in welded structures where rolling can be applied.

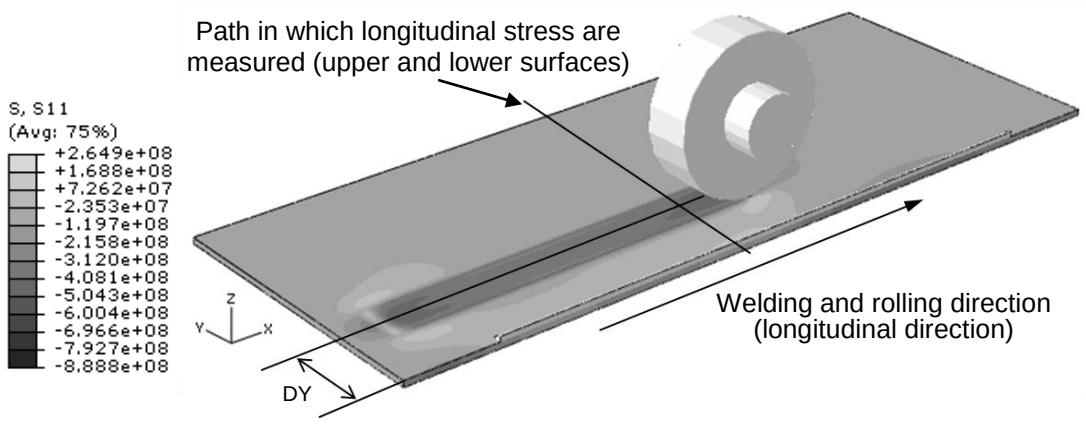

Figure 1: Longitudinal stress during pre-weld rolling. 100kN vertical load, and 55mm DY (stress in Pa).

1. Introduction

The stress generated by welding is well explained by Masubuchi [1]. Welding causes a large tensile stress in the longitudinal direction along the weld line. Since residual

stresses present in the plate are self-equilibrating, the tensile stress on the weld seam and surroundings cause a balancing compressive stress in the far field. This compressive stress can cause buckling distortion, particularly in thin material. Therefore, most techniques for reducing distortion focus on either reducing the magnitude or the width of the tensile stress which consequently reduces the compressive stresses that cause distortion.

Rolling to reduce residual stress has received relatively little attention in the literature. Kurkin *et al.* [2; 3] showed that a trailing roller behind the welding arc, reduced distortion in aluminium plates. More recently work by Altenkirch *et al.* [4] and Wen *et al.*[5] demonstrated results from experiments and numerical models of localized rolling on friction stir welds. The authors claimed that Post-Weld Direct Rolling (**PWDR**) on the weld line was the most effective method in terms of reducing residual stress and distortion.

Finally, Coules *et al.* [6] demonstrated how Pre-Weld Rolling (**PWR**) can reduce distortion. The advantage of PWR is that it could potentially be applied directly by the steel manufacturer before welding takes place. In this investigation either the top or bottom surfaces of the plate (relative to the side which is welded) was rolled prior to welding. Rolling on the bottom side with 200kN of vertical load at 55 mm from the weld centre line was found to give the greatest reduction in distortion. In this paper these results are compared with those from a numerical model, which helps to explain the reason for the reduction in measured distortion.

2. Method

2.1. Experiments

As reported by Coules *et al.* [6] experiments were performed using a rolling rig to roll, S355 mild steel, plates of size 500×200×4 mm. A controlled constant load and constant travel speed were applied during rolling. To constrain the plate during rolling and welding, vacuum clamps were used. A flat roller profile was used with 100mm diameter and 30mm contact width. The parameters used for rolling the plate are shown in Table 1. Note **DY** (Distance in Y direction) is defined as the distance between the edge and the centre of the roller's contact path (Figure 1). The butt welds were subsequentially produced with a Fronius TransPuls Synergic 5000 Gas Metal Arc Welding (**GMAW**) power supply. The welds were done in synergic mode with the parameters shown in Table 2. Thermocouples were used to determine the temperature field at distances of 10, 30 and 70mm from the weld centre line, on the upper surface. National Instruments CompactDAQ modular data acquisition unit was used for the temperature data acquisition, at a sampling frequency of 2Hz.

Finally, PWDR experiments were performed using the same equipment used for PWR. Steel S355 plates of 750×150×6mm size were welded with the parameters shown in Table 2. The material was rolled with a roller which matched the shape of the weld bead. The rolling parameters are shown in Table 1. Three samples were produced at each load.

Table 1: Rolling Parameters.

PWR			PWDR	
Speed [cm·min^{-1}]	Loading [kN]	Distance DY [mm]	Speed [cm·min^{-1}]	Loading [kN]
50	50	15	50	12.5
	100	25		25
	200	35		50
		55		
		80		

Table 2: Welding Parameters.

	Speed [cm·min^{-1}]	WFS [m/min]	Current [A]	Voltage [V]	CTWD [mm]	Filler wire diameter [mm]	Process
PWR	65	14.5	330	31.7	16	1	Pulsed
PWDR	50	16	360	32	13	1	Pulsed

2.2. Models

3D transient models were built in ABAQUS/Standard 6.9 to evaluate the PWR. The model was built in sequentially coupled thermal-mechanical mode. Temperature dependent material properties were used, which are shown in Figure 2. The thermal conductivity was artificially increased above the melting temperature to simulate the convective heat transfer into the weld pool [7]. Dimensional changes generated by solid phase transformation were taken into account through the thermal expansion coefficient. Isotropic hardening behaviour as well as annealing of the material were included in the model.

To reduce the number of nodes and consequently the computational time, linear brick elements, in the mechanical model, were implemented. On the other hand, quadratic brick elements were implemented in heat transfer models, since they performed better in terms of computational time and temperature distribution accuracy. In addition, different element sizes were used; a fine mesh in and around the welding seam and roller path; and coarser mesh in the rest of the plate as shown in Figure 3. The symmetric weld geometry meant only half weldment (one plate) was modelled.

A double ellipsoid Gaussian volumetric heat distribution was used to simulate the heat input from the GMAW process [8], as shown in Eq. 1. Where q_1 and q_2 represent the heat distribution ahead and behind the welding arc; a_1, and a_2, are the length in the front and rear ellipsoids; and b and c are the half of the width and depth of the ellipsoids respectively. Those values can be assumed about 90% of the weld pool size. f_f and f_r are fractional proportions of heat in the front and rear ellipsoids and their sums have to equal to 2. Q is the effective heat input in the experiments. The efficiency of the

arc was assumed to be approximately 83%. Forced convection (according to Newton cooling law) was applied in two different areas on the bottom plate, to simulate the thermal losses in that region, with two different coefficients, 425 and 250W·m^{-2}·K^{-1}, the former corresponding to the copper backing-bar and the latter to the aluminium vacuum clamps. Constant free convection coefficient (10 W·m^{-2}·K^{-1}) and emissivity (e = 0.8) were applied to the remaining external surfaces.

$$q_1(x,y,z,t) = \frac{6\sqrt{3}f_f Q}{a_1 bc\pi\sqrt{\pi}} . e^{-3\frac{[x+v(\tau-t)]^2}{a_1^2}} . e^{-3\frac{y^2}{b^2}} . e^{-3\frac{z^2}{c^2}}$$

$$q_2(x,y,z,t) = \frac{6\sqrt{3}f_r Q}{a_2 bc\pi\sqrt{\pi}} . e^{-3\frac{[x+v(\tau-t)]^2}{a_2^2}} . e^{-3\frac{y^2}{b^2}} . e^{-3\frac{z^2}{c^2}} \qquad \text{Eq. 1}$$

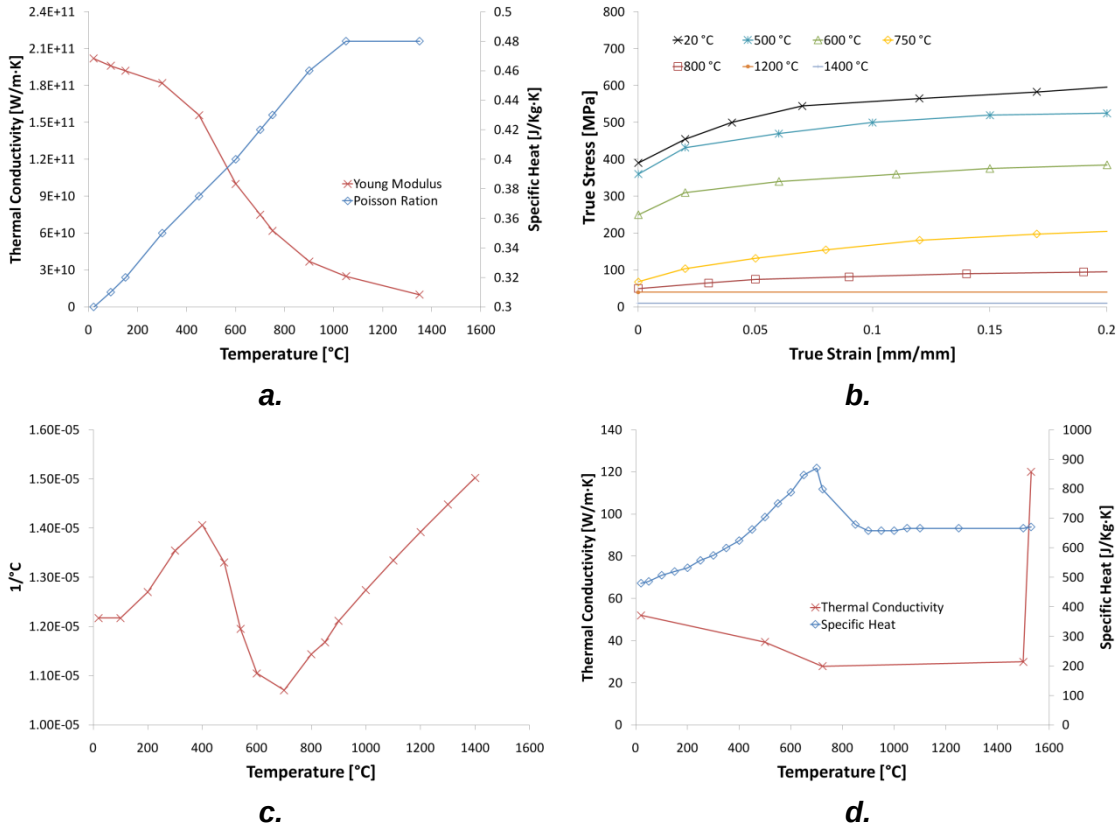

Figure 2: Temperature dependent material properties. ***a.*** Young modulus and Poisson ratio; ***b.*** flow stress; ***c.*** thermal expansion; and ***d***. thermal conductivity, and specific heat.

The model consisted of three steps: rolling, welding, and unclamping. All the nodes in the bottom plate were constrained vertically to simulate the action of the vacuum clamps, during rolling and welding, and were later removed during unclamping to allow distortion to take place. The right side surface was constrained against displacement in the longitudinal direction, while the plane opposite to the symmetry one (Figure 3) was restrained in the transverse direction. Symmetry boundary conditions, that constrain displacement in the transverse direction as well as rotation in the longitudinal and normal directions, were applied in the symmetry plane during welding, and were kept

during the unclamping step. One node remained fully restrained (encastre) on the middle of the symmetry plane on the weld root, during the unclamping step.

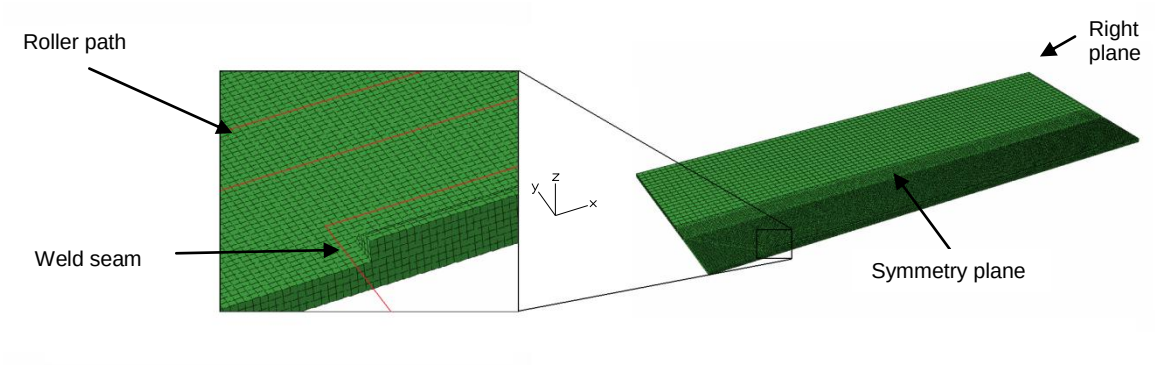

Figure 3: Mesh used in the analysis

Since the yield strength of the roller was larger than that of the workpiece, the former was modelled as an analytic rigid surface, while the plate as a deformable body. To simplify calculations and reduce computational time, no friction was assumed between roller and plate. The weld seam was deactivated during rolling and reactivated completely during the welding step. To avoid hourglass propagation (deformation with zero energy), hourglass control was implemented.

3. Results

3.1. Thermal field

A comparison of the numerical and experimental thermal profiles are shown in Figure 4 a. The peak temperatures predicted at 10 and 30 mm by the numerical model were 580 and 179°C respectively, which were slightly higher (30°C) than the experimental results. On the other hand, the temperature predicted by modelling at 70mm is almost identical to experimental result. The numerical model was also able to predict, with good agreement, the fusion zone, whose length was 39mm length against 36mm found in the experiments. The width of the weld bead in the top and bottom were almost identical being 10 and 2mm respectively for both the model and experiments. A plot of the thermal contours from the model is shown in Figure 4*b.*

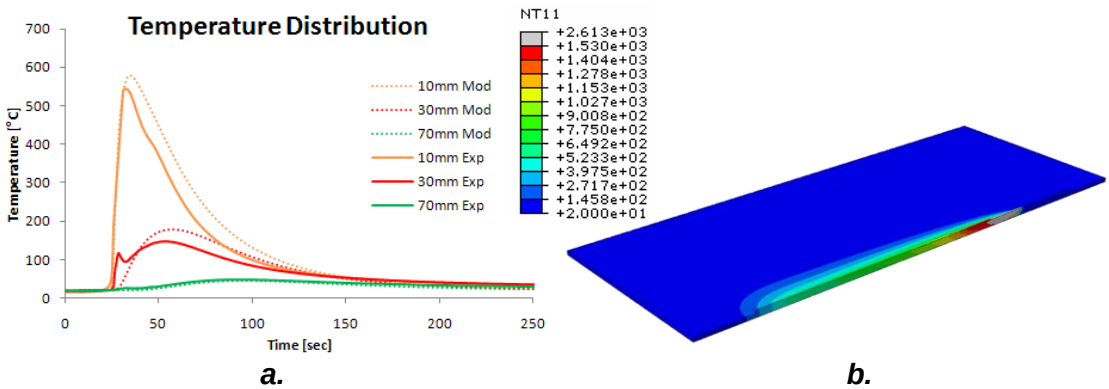

a. ***b.***

Figure 4: ***a.*** Comparison between experimental and numerical thermal profiles. ***b.*** Contour plot of temperature during welding (temperatures in °C).

3.2. Influence of welding on stress field

The longitudinal stress distribution after welding, in the as welded condition, before and after clamp removal is shown in Figure 5. The path along which the stresses are reported is shown in Figure 1. All measurements taken on the upper surface were along the plane z = 4mm and did not consider the weld bead reinforcement. Stresses in the upper and lower surfaces are almost identical as shown in Figure 5*a*, with a maximum tensile stress in the weld bead around 460MPa, which is over the yield point of the material, which is 390MPa. The stress distribution after unclamping is heavily affected by distortion as shown in Figure 5*a*. The upper surface has the larger stress release since the distortion tends to compress the top of the plate, as shown in Figure 5*b*. To have a more reliable method to compare stresses in the different rolling conditions only the stress distribution before unclamping will be analysed for the rest of this paper.

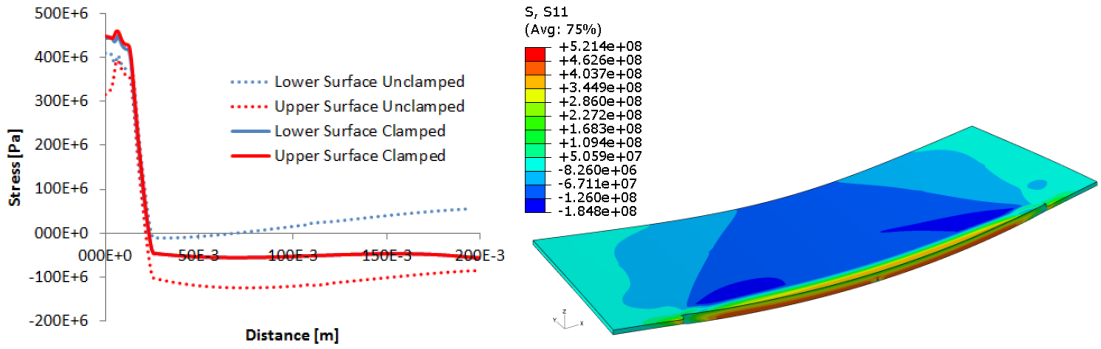

a. ***b.***

Figure 5: Longitudinal stress distribution in as-welded condition; ***a.*** clamped and unclamped; and ***b.*** contour plot, including deformed shape, with a scale factor of 5 to magnify distortion (stress in Pa)

3.3. Influence of rolling on stress field

The stress distribution during (while the roller is in-line with plotting path) and after rolling are shown in Figure 6. During rolling tensile stresses are developed on the edge

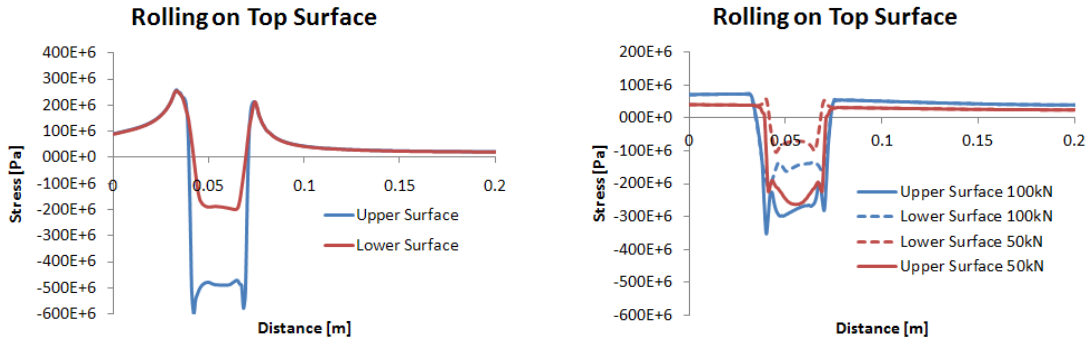

a. ***b.***

Figure 6: Longitudinal stress distribution when ***a.*** the roller is in-line with the plotting path with a rolling load of 100kN; and ***b.*** after rolling with loads of 100 and 50 kN on the upper surface. In both cases the roller is 55mm from the centreline (DY).

where the material was subsequently welded, and also compressive stresses were generated under the region which was rolled (Figure 6*a.*). This phenomenon is the basis of the In-Situ Rolling Tensioning technique (**ISRT**) described by Wen *et al.* [5] and Altenkirch *et al.* [4]. After rolling residual tensile stress is present along the edge (which will be welded). Figure 6*b* shows how the tensile (along the weld edge) and compressive (underneath the roller path) stresses generated by the roller process depend on the rolling load. A higher load produces higher stresses.

3.4. Influence of pre-welded rolling

The numerical and experimental distortion results are shown in Figure 7. Since the mesh density is not uniform throughout the geometry, the average displacement was determined by discretisation of the surface in equal square areas. The results show a partial agreement between experimental and modelled results. The model of the as-welded condition seems to underestimate the distortion having about 63% of the average distortion found in the experiments. On the other hand, PWR seems to have, in both experiments and models, a negative effect on distortion when applied to the top surface.

The most significant distortion reduction found in the experimental results was rolling on the bottom with a load of 200kN, 55mm from the welded edge, which achieved a distortion reduction of 38%. The numerical model predicted 43% distortion reduction with these parameters. However, since the yielding point of the material at room temperature on the model was lower than on real plates (around 22% lower) a direct comparison is not possible.

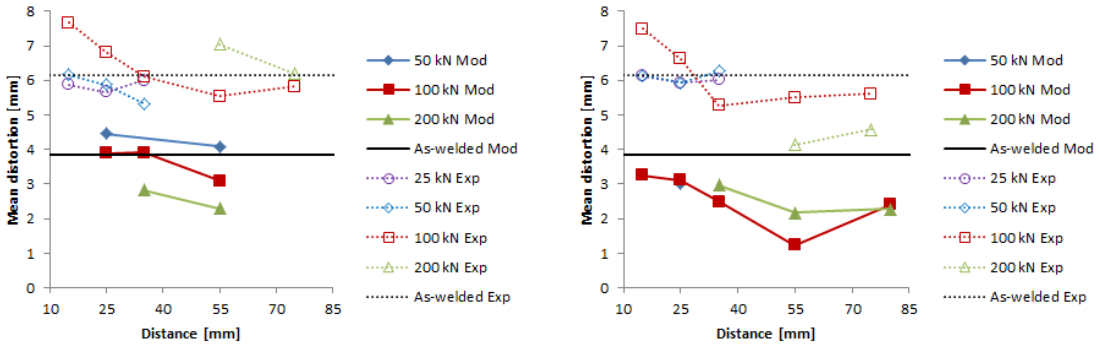

Figure 7: Mean distortion after PWR. ***a.*** Rolling on the top surface and ***b.*** bottom surface.

Longitudinal residual stresses before unclamping in PWR are plotted in Figure 8. Rather than reducing peak tensile stress in and around the weld bead, the rolling affects the distribution of stresses in the far-field. The best results, in terms of distortion reduction (68%), were obtained for rolling in the bottom surface with 100kN load at 55mm DY (Figure 8*a.*). The variation in stresses between the top and bottom surfaces of the rolled region is likely to induce bending distortion. When rolled on the bottom surface, the bending distortion opposes that caused by the welding process. When applying the same parameters to the top surface, the stress distribution is similar (Figure 8*b*), however the buckling distortion induced by the roller adds to that from the

welding process. Rolling in the bottom surface closer to the welding edge (15mm DY) was also studied, showing a slight reduction of the width of the tensile peak. However, the magnitude of the tensile peak was increased by 100MPa over the as-welded condition, as shown in Figure 8*c*.

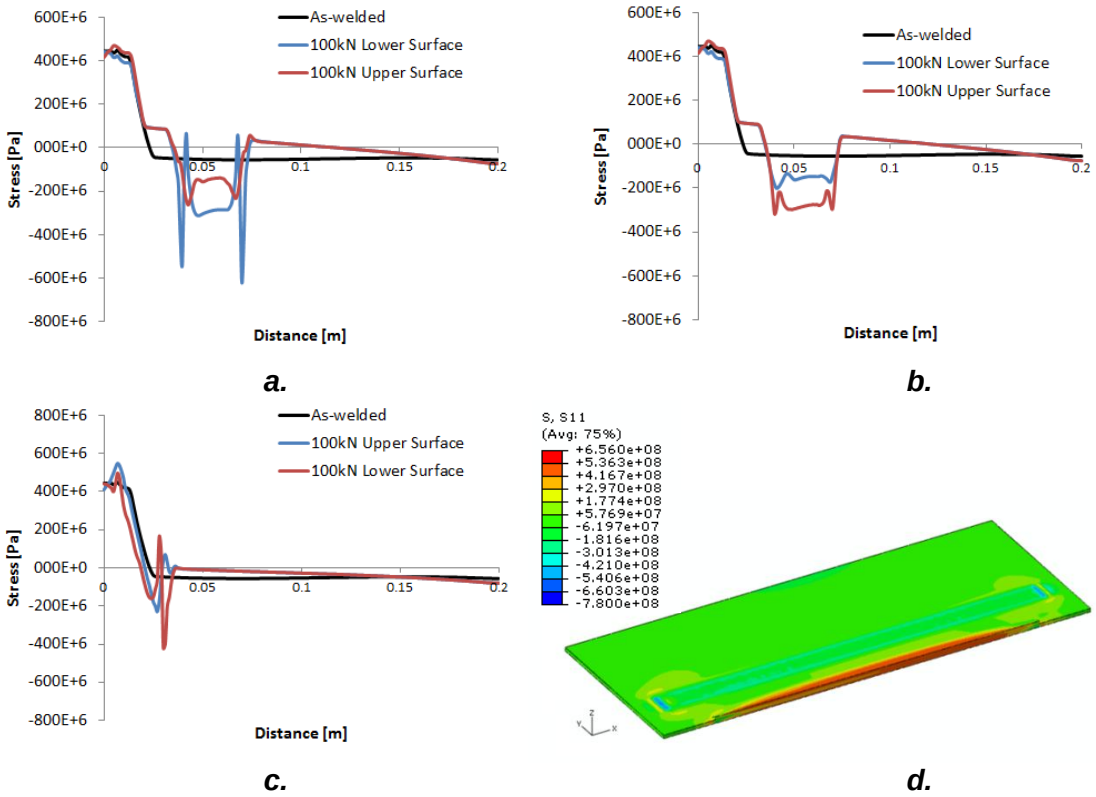

Figure 8: Longitudinal residual stresses after PWR and before unclamping; ***a.*** rolled on the bottom surface at 55 mm DY with 100kN load; ***b.*** as for *a*. but rolled on the top surface; ***c.*** as for *a*. but at 15mm DY. ***d.*** Contour plot of longitudinal stress after PWR before unclamping, rolled on the bottom surface with 100kN load at 55mm DY (stress is Pa).

3.5. Influence of post-welded direct rolling

Preliminary PWDR were performed with encouraging results. Mean distortion in experimental results after PWDR is shown in Figure 9. After rolling, with 50kN of vertical load, virtually flat plates were obtained with a mean distortion under a millimetre, which is more than a 70% distortion reduction. The results seem to be coherent with those published by Altenkirch *et al.*[4] and Wen *et al.*[5]. In comparison with PWR results, PWDR seems to be more repeatable, with smaller variation in the results. Unlike Altenkirch's results, there is no particular benefit of increased rolling load. It is believed that a rolling load of 12.5kN is sufficient to reduce the tensile stress in the weld region below that which would cause significant distortion.

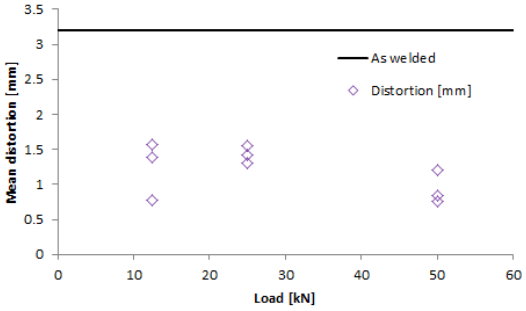

Figure 9: Mean distortion on experiments after PWDR

4. Conclusions

Numerical models of PWR on mild steel were conducted using different loads and distances DY, from the weld centreline. A comparison with experimental results was done, and also preliminary PWDR results were presented. In this work we demonstrated that:

- PWR produces a region of compressive stress under the roller path and a balancing tensile stress along the edge to be welded (Figure 6).
- The greatest reduction in the model's prediction of distortion with PWR was when the material was rolled on the bottom surface at a distance of 55mm from the weld line, using a load of 100kN. The experiments required higher load (200kN). Inaccurate values of the materials properties were the most likely cause of the discrepancy.
- The model predicted reductions in distortion which were similar to those observed experimentally.
- The likely mechanism for the reduced distortion with PWR is the addition of stresses that cause bending, which opposes that caused by the welding process.
- PWDR seems to be more consistent and the preliminary results are encouraging. This method produced a virtually flat palate with an average mean distortion reduction of over 70%.

5. Acknowledgements

The authors would like to acknowledge funding for this project from Tata Steel Europe and from the EPSRC under grant no. EP/G014132/1.

6. References

[1] Masubuchi, K. (1980), Analysis of welded structures, 1st ed, Pergamon Press.

[2] Kurkin, S. A., Anufriev, V. I. and Milekhin, E. S. (1980), "Improving the Mechanical Properties of Welded Joints in the AMg6 Alloy by Plastic Deformation During Arc Welding", Weld.Prod., vol. 27, no. 3, pp. 20-24.

[3] Kurkin, S. A., Anufriev, V. I. and Baumana, N. E. (1984), "Preventing Distortion of Welded Thin-Walled Members of AMg6 and 1201 Aluminum Alloys by Rolling the

Weld With a Roller Behind the Welding Arc", Weld.Prod.(USSR), no. 10, pp. 52-55.

[4] Altenkirch, J., Steuwer, A., Withers, P. J., Williams, S. W., Poad, M. and Wen, S. W. (2009), "Residual stress engineering in friction stir welds by roller tensioning", Science and Technology of Welding and Joining, vol. 14, no. 2, pp. 185-192.

[5] Wen, S. W., Colegrove, P. A., Williams, S. W., Morgan, S. A., Wescott, A. and Poad, M. (2010), "Rolling to control residual stress and distortion in friction stir welds", Science and Technology of Welding and Joining, vol. 15, no. 6, pp. 440-447.

[6] Coules, H. E., Cozzolino, L. D., Colegrove, P. and Wen, S. W. (Under Review), "The effect of pre-weld rolling on distortion and residual stress in fusion welded steel plate", June 26-28, 2010.

[7] Michaleris, P. and Debiccari, A. (1997), "Prediction of welding distortion", Welding Journal (Miami, Fla), vol. 76, no. 12, pp. 172-s.

[8] Goldak, J. A., Chakravarti, A. and Bibby, M. (1984), "A new finite element model for welding heat sources", Metallurgical Transactions B, vol. 15, no. 2, pp. 299-305.